Environmental Science Nano

Ion Selective Nano-mesh Electrode for Long-term Continuous Monitoring of Wastewater Quality Fabricated Using Template-Guided Membrane Immobilization

Journal:	*Environmental Science: Nano*
Manuscript ID	EN-ART-10-2021-000966.R1
Article Type:	Paper

Environmental Significance Statement

The long-term continuous monitoring of water quality in natural environments and engineering contexts using ion-selective sensors requires electrochemical stability, mechanical strength and extended lifespans of the sensors. Due to their general vulnerability, nano material-based sensors have been limited to short-term and lab-based applications. This study deployed an innovative template-guided nano-mesh (TN) technique to fabricate NH_4^+ ion-selective electrode (ISE) sensors using a nano-sized nickel electrode substrate. The resulting TN-ISE sensors exhibited enhanced electrochemical stability, higher selectivity and longer lifespans compared to a regular carbon nano-tube (CNT) ISE sensors. This was validated through 100-day test in clean water solutions and 15-day tests in wastewater, the longest test periods reported for nano material-based water sensors. The technology platform presented here for the trapping and stabilization of ion selective membranes in nano materials is suggested to be suitable for the fabrication of a broad spectrum of durable ISE sensors that rely on chemosensor matrixes laminated on nano-scale electrode substrates.

Ion Selective Nano-mesh Electrode for Long-term Continuous Monitoring of Wastewater Quality Fabricated Using Template-Guided Membrane Immobilization

Tianbao Wang,[a] Can Cui,[b] Yuankai Huang,[a] Yingzheng Fan,[a] Zhiheng Xu,[a] Logan Sarge,[a] Christos Bagtzoglou,[a] Christian Brückner,[c] Puxian Gao,[b] Baikun Li*[a]

[a] Department of Civil & Environmental Engineering, University of Connecticut, Storrs, Connecticut 06269, United States. Email: baikun.li@uconn.edu

[b] Department of Materials Science and Engineering, University of Connecticut, Storrs, Connecticut 06269, United States

[c] Department of Chemistry, University of Connecticut, Storrs, Connecticut 06269, United States

Abstract

Ion selective electrode (ISE) sensors have been broadly applied for real-time *in situ* monitoring of ion concentrations in water environments. However, ISE sensors suffer from critical problems, such as ionophore leaching, water-penetration, poor electrochemical stability, and resulting short life spans. In this study, a template-guided membrane matrix immobilization strategy was pursued as a novel ISE sensor fabrication methodology to enhance its sensing characteristics and longevity. Specifically, nano-porous anodized aluminum oxide (AAO) was used as the template for an NH_4^+-specific ISE sensor. A nano-porous nickel mesh eventually replaced the template and formed a compact, high-surface juncture with the NH_4^+ ion-selective membrane matrix. The resulting template-guided nano-mesh ISE (TN-ISE) sensor displayed enhanced electrochemical stability (i.e., capacitance increased by 50%, reading drift reduced by 75%) when compared to a regular single-wall carbon nanotube (SW-CNT) ISE sensors used as standard. The interface between the nano-mesh electrode and the ion selective membrane matrix was compact enough to prevent water influx at the electrode interface. This minimized ionophore leaching and increased the mechanical integrity of the TN-ISE sensor. The practical advantages of the novel sensor were validated via long-term (360 hours) tests in real wastewater, returning a small average error of 1.28% over this time. The results demonstrate the feasibility of the template-guided nano-mesh design and fabrication strategy toward ISEs for long-term continuous monitoring of water or wastewater quality.

1. Introduction

Real time *in situ* monitoring of inorganic and organic contaminants in water is of vital importance for water and wastewater treatment plants (WTP and WWTP) since water quality is highly dynamic and heterogenous at spatial-temporal levels. Conventional discrete sampling and off-line laboratory-based analysis cannot fulfill such requirements.[1] Solid state ion selective electrode (S-ISE) sensors of high selectivity to specific ions (e.g., ammonium, nitrate, phosphate, etc.) have the advantage of delivering fast responses to dynamic concentration changes, all in small sensor dimensions. This enables their convenient and wide deployment to monitor ion concentrations in water and wastewater.[2-5] However, S-ISE sensors suffer from short life spans due to sensor reading drifts (i.e., electrochemical instability) and mechanical failure, especially in wastewater with drastic fluctuations of water quality and quantity.[6, 7] Real time *in situ* monitoring of NH_4^+ in wastewater, for example, is critical for nitrogen removal in WWTPs. This need requires NH_4^+ sensors to be submerged in wastewater for (at least) several weeks to several months. Sensors with poor reading accuracy and short lifespan incur frequent re-calibrations, maintenance and replacement, leading to labor-intensive and costly operation.[8, 9] Thus, the mitigation of S-ISE sensor reading drifts and prolonging sensor lifespan are critical for S-ISEM sensors to become practical and economical long-term solutions to monitor water quality in WTP and WWTP.

Sensor reading drift is the fluctuation of sensor signals (e.g. potential (mV) readings of S-ISE sensors) over time ($\Delta E/\Delta t$) due to slow equilibrium processes at the interface between the electrode and the ion selective membrane matrix[10] that may be induced by the polarization of the electrode over time. In fact, all electrode surfaces are getting polarized to some extend over time due to a dielectric discontinuity at the electrode-electrolyte interface (Eq. 1):[11]

$$E = E^0 + i\left(R + \frac{t}{C}\right) (1) \quad \text{(Eq. 1)}$$

Where E is the potential of electrode, i is current, R is the resistance, t is the time, and C is the capacitance.

A sufficiently high electrode capacitance is necessary for a satisfactory potential stability to minimize the reading drift ($\Delta E/\Delta t$). Previous studies enlarged the capacitance of the electrodes of ion selective electrodes by using nano-porous materials due to their high pore density (1×10^8 to 1×10^{13} cm^{-2}).[7, 12] The double-layer capacitance could also be improved by the enlarged contact surface area between the nano-porous electrode and the ion selective membrane matrix. For example, nano-scale materials, such as single-walled carbon nanotubes (S-CNT),[13] nano-porous gold films,[6] or graphene[14] were used to achieve high double-layer capacitances. However, these nano material-based electrodes also suffer from drawbacks, including poor processability caused by the insolubility or poor solubility of their components and particularly weak adhesion of ISE polymer matrix to the rough and loose interface of CNT.[6] In addition, lab-based ISE sensors are generally being fabricated by drop casting of an ionophore polymer matrix onto the electrode surface. This frequently results in a loose contact between the polymer and surface, causing numerous interspace defects and correspondingly higher chances of the water layer formation between the membrane matrix and the electrodes (Fig. 1a). Eventually, this results in sensor reading drifts and sensor mechanical failures over time.[15, 16]

This study addresses the improvement of the contact interface between membrane matrix and electrode using a template-guided membrane matrix immobilization technique based on an anodized aluminum oxide (AAO) template. Because of the excellent compatibility of AAO templates with different fabrication methodologies,[17-19] they have been extensively applied in the

manufacture of complex nanostructured devices.[20-22] Using this technique, we expected to increase the interface area of tight ionophore matrix-electrode contact in ISMs. This approach proved to be successful. Thus, this contribution describes using an AAO template in the construct ion of a robust ISM for long-term NH_4^+ detection. Its superior characteristics are demonstrated in direct comparison to a more traditionally manufactured ISE using the same chemosensor matrix. The enhanced capacitance of the nano-mesh ISE sensors and its reduced leaching of the chemosensor alleviated issues of sensor reading drafts. The results presented here suggest this technology for the realization of long-lived ISMs (demonstrated here for NH_4^+ but potentially also applicable to other ions) for real time *in situ* monitoring of WTP and WWTP.

2. Methods and materials

NH_4^+ ISE Sensor fabrication

NH_4^+ ion selective membrane matrix (S-ISM cocktail): Composed of a cocktail of NH_4^+ ionophore (Nonactin), 5.0 wt. %, dibutyl sebacate (decanedioic acid dibutyl ester, DBS), 68.0 wt %, potassium tetrakis(4-chlorophenyl)borate (KT4ClPB), 2.0 wt %, and polyvinyl chloride (PVC, average $M_w \sim 43000$), 25.0 wt %, all components obtained from Sigma-Aldrich. The cocktail (100 mg in total) was dissolved in tetrahydrofuran (THF, 500 µL) and then mixed ultrasonically for 10 min, following the protocols previously reported.[8, 23, 24]

Graphite-based ISE sensors and single-wall carbon nanotube-based ISE sensor (electrodes used as controls): An aqueous suspension (10^{-2} wt % in acetone) of single-wall carbon nanotubes (SW-CNT) were mixed ultrasonically for 1 h. The surface of the working electrode (same ET077-40 Zensor electrode strip, 3 mm diameter) (Fig. 1f) was first covered with this SW-CNT suspension

(4 μL) to form the ion-to-electron transducer layer; it was air-dried for 10 s. Then the NH_4^+ S-ISM cocktail solution (4 μL) was carefully drop-cast onto the SW-CNT layer (Fig. 1a); the NH_4^+ sensors were then air-dried over 48 h under ambient conditions to form the S-ISM solid layer on the working electrode surface. Additionally, a graphite-based ISE sensors (GC ISE) used as another control sensor was fabricated using the same NH_4^+ S-ISM cocktail solution (4 μL) on the same electrode strip but without the layer of SW-CNT.

SW-CNT ISE sensors were used as the control in this study because they have been well developed and are readily accessible. Previous studies had found that carbon-based materials (e.g., three-dimensionally ordered macroporous carbon[25], colloid-imprinted mesoporous carbon[26], single wall carbon nanotube[27-29]) as the solid contact displayed great improvement for potential stability, reproducibility, minimizing potential reading drift[30]; they were thus deemed to be excellent benchmarks.

Template-guided Ni nano-mesh (TN) ISE sensor: The pore size of the AAO template is adjustable in the range of 5 - 500 nm and a pore density between 1×10^8 and 1×10^{13} cm^{-2}.[31, 32] Here, we aimed to trap the ion selective membrane matrix (ISM) inside nanotubes of the entire nano-mesh and maximize the contact surface area. Thus, 300 nm was selected as the pore diameter (Fig. 1c-1e). Specifically, the Al foils went through the first-anodization in a 5 wt % phosphoric acid under a constant voltage of 160 V for 10 min. The as-prepared anodized Al was dissolved in chromic acid (1.5 wt % $K_2Cr_2O_7$ in 96% H_2SO_4) and 6 wt % phosphoric acid at 60 °C for 5 h. Then the second anodization was carried out in the same condition as the first, for 3 h, to form the AAO template, through which the anodized Al expanded to around 300 nm in diameter and 20 μm in depth (Fig. 1c). Subsequently, the remaining Al on backside was dissolved by an etching solution containing 10 g $CuCl_2$, 200 mL HCl (37.0%), and 200 mL DI water to expose the AAO template. Then, the

AAO template was coated with an Au layer (20 nm thickness) using sputtering (Safematic, CCU-010 HV). The NH_4^+ ISM cocktail was filled into the template via capillary attraction at room temperature for 12 h. Subsequently, the AAO template was removed using a phosphoric acid solution (3 wt%) and the ISM matrix skeleton (blue tubes in Fig. 1b) were immerged in a standard three electrode cell (as the cathode) and the electrochemical deposition of a thick film of elemental nickel (Ni) nano-mesh proceeded at a constant current of 10.0 mA/cm^2 in an aqueous electrolyte (0.38 M $NiSO_4$, 0.12 M $NiCl_2$, and 0.5 M H_3BO_3) for 2 h. The scanning electron microscopy (SEM) image (Fig. 1d) shows the Ni nano-mesh holding the NH_4^+ ISM polymer matrix. Using acetone to dissolve the ISM matrix obtained the pure Ni nano-mesh (the SEM picture in Fig. 1e) for electrochemical tests.

Characterization for the template-guided nano-mesh (TN) electrode

Nano-mesh materials and NH_4^+ ISM sensors were characterized using a Verios 460L SEM (Fig. 1c: the cross-section image of AAO template; Fig. 1e: the cross-section image of Ni nano-mesh filled with NH_4^+ ISM). In order to obtain capacitance measurements for the template-guided Ni nano-mesh only (without the interference of NH_4^+ ISM), we dissolved the matrix in acetone and washed it away, revealing the pure Ni nano-mesh (Fig. 1d). The measurements for the capacitance of template-guided nano-mesh electrode was performed by cyclic voltammetry (CV) and electrochemical impedance spectroscopy (EIS) using a CHI 660D potentiostat. The CVs were performed at potential range from 0-0.1 V and a scan rate range of 0.005-0.1 V/s; electrolyte was an aqueous solution of 0.1 M KCl (ACS reagent, Sigma-Aldrich). The EIS tests were carried out at 0.1, 0.15, and 0.2 V vs Ag/AgCl, at frequencies ranging from 100 kHz to 100 Hz. The electrolyte was an aqueous solution of 0.1 M KCl (ACS reagent, Sigma-Aldrich). The EIS results were fitted

using the ZView2 software. Every nano-mesh sample test was carried out in triplicate, with average data presented.

Electrochemical tests for the template-guided nano-mesh ISE (TN-ISE) sensor

Chronopotentiometry (in an aqueous solution of 0.1 M KCl) was used to determine the difference in the potential (mV) stability of two types of ISE sensors, the SW-CNT ISE sensor (as a reference) and the TN-ISE sensor using an electrochemical workstation (CHI 660D). The chronopotentiometry tests were then carried out via alternate input current from +1 nA for 60 s, then -1 nA for 60 s. A small reading drift after switching the current direction indicates good potential stability.[33]

In addition, water layer tests were carried out for both S-CNT ISE sensor and TN-ISE sensors to compare their potential (mV) stability. Firstly, both sensors were soaked in an aqueous 0.1 M NH_4Cl solution (primary target ion NH_4^+ solution) for 1 h at ambient T. Subsequently, both sensors were switched to an aqueous 0.1 M NaCl solution (containing the interfering Na^+ ion for 2.5 h). Finally, both sensors were put back to 0.1 M NH_4Cl solution and immersed for 6.5 h to equilibration. The potential (mV) readings of both sensors were recorded using an electrochemical workstation (CHI 660D). Small reading disparities before and after the solution switch indicated a high stability. Every sample test was carried out in triplicate, with average data presented.

UV-visible spectrophotometry for quantification of component leaching process

To determine the prevention of leaching by nano-mesh material, S-CNT ISE sensor and TN-ISE sensors were examined side-by-side by immersing in DI water for 100 days. The DI water for both sensors were measured using the spectrophotometer daily to evaluate the leaching amount of KT4ClPB. For each group of sensor samples, three duplicated pieces were fabricated and observed.

Specifically, all the sensor samples were soaked in a sealed bottle (volume: 6 mL) with 3 mL de-ionized (DI) water. The component leached out from the sensor membrane matrix into the DI water over time (100 d); this was measured using spectrophotometry (Varian Cary 50) in the wavelength range from 800 to 200 nm. Based on experiment result, the lipophilic salt KT4ClPB leached out of the membrane to aqueous sample constantly in these 100 days. Even though the aqueous sample (3mL DI water) was saturated with KT4ClPB in the middle of 100 days, the constant leaching amount of KT4ClPB could still be determined as suspension. A bare sensor strip (ET077-40 Zensor, graphite as the substrate) without any chemical deposition was used as the control sensor in this leaching test. Meanwhile, the sensitivity (slope) of each sensor was measured regularly for 100 d to establish the relationship between the leaching and the sensor sensitivity. Details about the UV-visible spectrophotometry for the leaching tests are described in Text S1.

Continuous long-term test for the template-guided nano-mesh ISE (TN-ISE) sensors in wastewater

The comparative performance of the S-CNT ISE and TN-ISE NH_4^+ sensors were also evaluated in real wastewater. The wastewater was taken from the effluent of the UConn Wastewater Treatment Plant ($[NH_4^+]$ = 2.5 mg/L, chemical oxygen demand (COD): 10-20 mg/L). Both sensors were immersed in a batch-mode beaker containing 1 L wastewater for 360 h (15 d) consecutively. It was stirred by a stir bar with constant rotation rate (25 rpm) to simulate the turbulence in real-world wastewater systems. The potential readings (mV) of both sensors were recorded every 5 s using an electrochemical workstation (CHI 660D). The test was performed in a fridge at 0 ℃ to inhibit microbial activities that could cause variations of nitrogen concentration. In addition, the wastewater was shielded from light and air exchange was inhibited by sealing of the beaker via film. The sensors were briefly taken out of wastewater every 30 h for a sensitivity check (i.e. slope

value) carried out using standardized (2, 4, 8, 16, 32, and 64 mg/L) NH_4Cl solutions. Additionally, the long-term potential readings (mV) of both types of ISE sensors were converted to NH_4^+ concentrations (mg/L) based on the sensitivity curves. Throughout the 360 h duration of the test, sensor reading correction was performed five times in total based on the results of sensitivity check every 60 h. NH_4^+ concentration derived from both types of ISE sensors were then validated against traditional off-site Salicylate Method (Method 10031) using a Hach DR2800 every 60 h. In addition, to examine the response of the nano-mesh ISE sensors to transient shocks occurring in water/wastewater, a shock test was conducted at the end of the 360-hr test by adding 10 μL of concentrated NH_4Cl solution (100 g/L) to wastewater.

3. Results and discussion

3.1 Design principles and construction of the template-guided nano-mesh (TN) electrode

We chose to address an improvement of the tightness of the contact interface between membrane matrix and electrode using a template-guided membrane matrix immobilization technique that is based on AAO templates (Fig. 1b). This material was chosen because of the excellent compatibility of AAO templates with different fabrication methodologies[17-19] involving multiple nanostructures, such as nanoparticles, nanowires, or nanotubes.[20-22] Porous AAO has a high pore density (1×10^9 to 1×10^{12} cm^{-2}), an even pore distribution, and the pore size can be adjusted in the range from 5 to 500 nm; this enables the selection of a pore size compatible for a specific ion selective membrane (ISM).[12, 32, 34] Since AAO templates with hole sizes smaller than 300 nm are appropriate for nano wire fabrication,[35] we built an AAO template with hole diameters of 300 nm by anodizing Al foil (Fig. 1c). Following the deposition of an electrically conducting Au layer onto the

aluminum oxide template by sputtering techniques, the ISM solution filled the porous AAO template. After solidification by polymerization of the ISM matrix, one overlayer of ISM was left. Then the template structure was removed and, by growing on the thin Au layer that was retained, electrodeposited Ni ions replaced the template to form a nano-mesh. This was in intimate contact between with ISM matrix (Fig. 1d-1e). The nano-mesh electrode with ISM thusly obtained was exceptionally compact. As we will show below in detail, this prevented water invasion and membrane matrix detachment, prevented sensor leaching, and led to an enhanced capacitance of the nano-mesh ISE sensor. The combination of these effects alleviated sensor reading drafting issues.

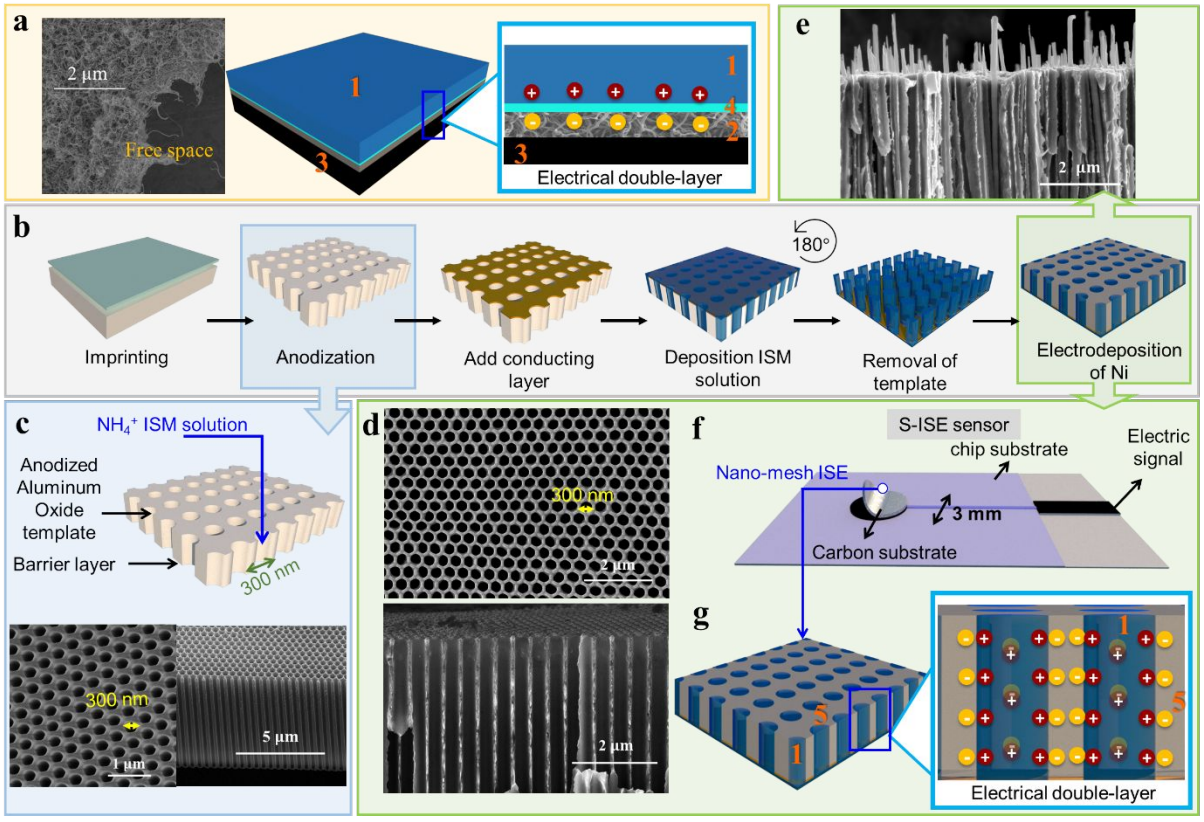

Fig.1 (a) SEM (left) and schematic cross-section view of S-CNT ISE sensor with the diagram of electrochemical double-layer. 1: ion selective membrane matrix; 2: single wall carbon nanotube (S-CNT); 3: carbon electrode surface; 4: water layer in the instable interface between ion selective

membrane matrix and S-CNT. (b) Schematic of the fabrication process for template-guided nano-mesh ISE sensor (TN-ISE). Left to right: imprinting on an Al foil; anodization on the imprinted Al foil to form anodized aluminum oxide (AAO) template; adding a layer of Au as conducting layer; depositing ion selective membrane solution on the template; reversing sample and removing the template; electrodepositing elemental Ni starting the Au layer and embedding the solid ion ISM matrix. (c) Structural diagram and corresponding SEM image of AAO template. (d) SEM image of the pure template-guided nano-mesh electrode (after removing ion selective membrane by acetone). (e) SEM image of the template-guided nano-mesh ISE sensor. (f) Layout of chip substrate for ISE sensor. (g) Diagrammatic cross-section view of template-guided nano-mesh ISE sensor: 5: Ni nano-mesh as electrode**.**

3.2 Electrochemical characterization of the template-guided nano-mesh (TN) electrode

A high double-layer capacitance of an electrode is expected to enhance the long-term potential (mV) stability of an ISE sensor (Eq. 1), and a large surface area results in a high electrochemical double-layer capacitance (Eq. 2):

$$C = \varepsilon_0 \cdot \varepsilon \cdot A/d, \qquad \text{(Eq. 2)}$$

where C is the double-layer capacitance, ε_0 and ε are the permeability of free space and dielectric constant of the medium, A is the plate area, and d is the inter-plate distance.[6]

The surface area of a nano-mesh electrode was considerably enlarged due to its nano-porous structure (Fig. 1g). The electrochemical double-layer capacitance of a nano-mesh electrode surface was determined by measuring the non-Faradaic capacitive current associated with double-layer charging from repeated cyclic voltammetry (CV) scans.[36, 37] The potential range of 0-0.1 V was used because no obvious electrochemical features corresponding to a Faradaic current was

observed within this voltage window (Fig. 2a). Thus, all the current measured in this non-Faradaic potential region is assumably caused by double-layer charging. The 0.1 V potential window was centered at the open circuit potential (OCP: 0.05 V, Fig. 2a) of the three-electrode system.

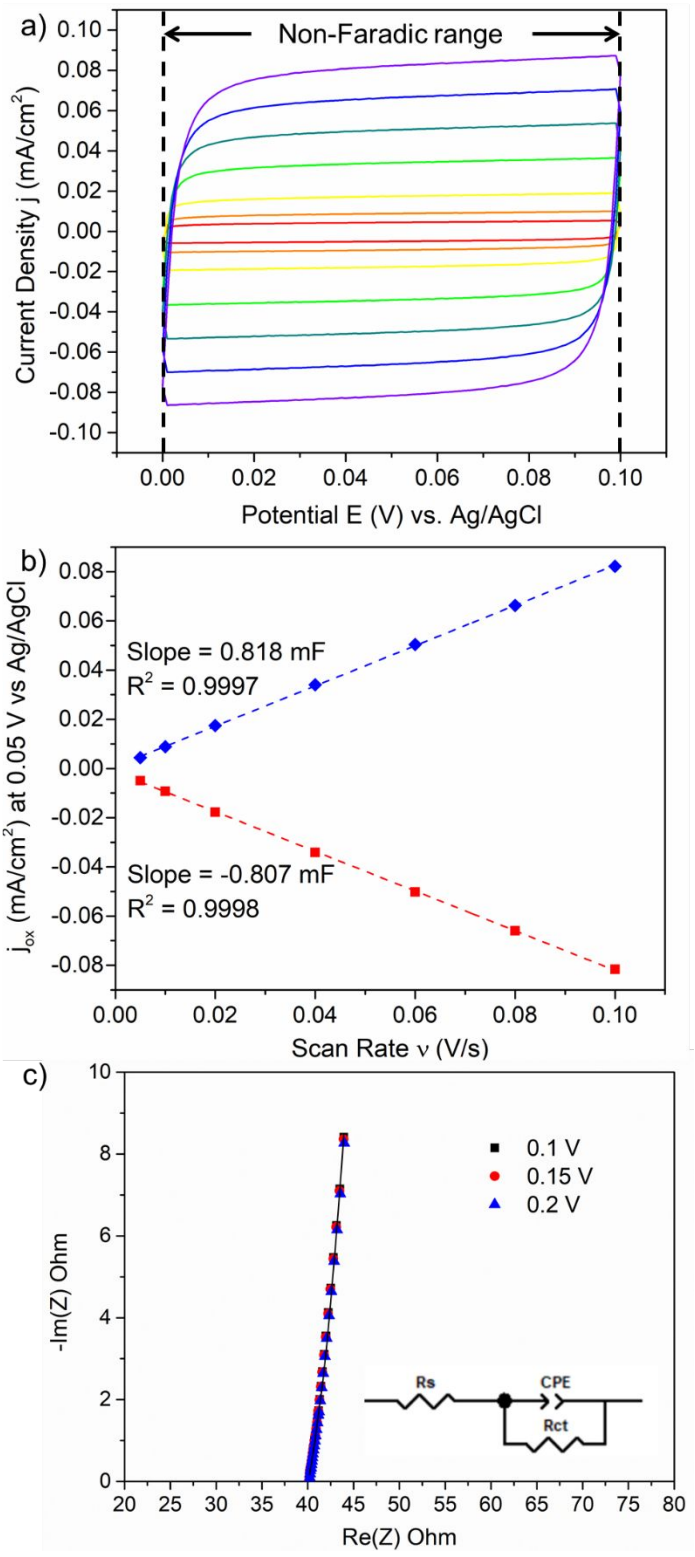

Figure 2. Double-layer capacitance measurements for template-guided nano-mesh electrode (TN-ISE) from voltammetry and EIS in 0.1 M KCl. (a) Cyclic voltammogram were taken in a non-

Faradaic region at following scan rates: 0.005 (red line), 0.01 (orange line), 0.02 (yellow line), 0.04 (green line), 0.06 (cyan line), 0.08 (blue line), 0.10 (purple line) V/s. The working electrode was held at each potential vertex for 10 s before the beginning the next sweep. (b) The anodic (blue dot) and the cathodic (red dot) charging currents were recorded at 0.05 mV vs Ag/AgCl, then were plotted as function of scan rate. (c) Nyquist plots of nano-mesh electrode at 0.1 (black square), 0.15 (red circle), and 0.2 V (blue triangle) vs Ag/AgCl measured from EIS in the frequency range 100 kHz to 100 Hz. The inset represents the Randles curcuit.

The double-layer current (i_c) is equal to the product of the scan rate (ν) and the electrochemical double-layer capacitance (C_{DL}) (Eq. 3 [36, 38]).

$$i_c = \nu \cdot C_{DL} \quad \text{(Eq. 3)}$$

The dependence of the current on the scan rate in this region is linear (Fig. 2b), consistent with capacitive charging behavior. Accordingly, the slope of straight lines of i_c as a function of ν (Fig. 2b) is equal to the electrochemical double-layer capacitance. The final electrochemical double-layer capacitance (812.5 μF) was calculated from the average of the absolute value of slopes. This value is significantly enhanced compared with other electrodes used as ISE sensors (e.g., carbon nanotube-based sensors 60 μF;[3] gold nanocluster-based sensor 118 μF;[6] graphene-based sensor 78 μF,[36] etc.).

The double-layer capacitance was also measured using EIS in the non-Faradaic region from 0-0.2V. The Nyquist plot of the electrochemical impedance in a non-Faradaic region was obtained between 100 Hz and 100 kHz for a nano-mesh electrode (Fig. 2c). The impedance spectrum of the nano-mesh electrode displays a capacitive line with a slope of near 90° in the low-frequency region

with the absence of a semicircle in the high-frequency region, indicating that these interfacial ion/electron transfer processes were fast at the interface between the nano-mesh electrode and KCl solution. Besides, the potentials of 0.1, 0.15, and 0.2 V fall in a potential region (Fig. 2c) in which no Faradaic processes were observed. Under non-Faradaic conditions, the electrochemical system was approximated by the modified Randles circuit (the inset figure, Fig. 2c), where R_s is the solution resistance, CPE is a constant-phase element related to the double-layer capacitance, and R_{ct} is the charge-transfer resistance from any residual Faradaic processes. The double layer capacitance C_{DL} is determined according to Eq. 4 [39, 40].

$$C_{DL} = \left[Q_0\left(\frac{1}{R_s} + \frac{1}{R_{ct}}\right)^{a-1}\right]^{1/a} \quad \text{(Eq. 4)}$$

Where Q_0 is a constant with units of F s^{a-1} and a is related to the phase angle of the frequency response. In this study, $Q_0 = 1.078$ F s^{a-1}, $R_s = 40.26\ \Omega$, $R_{ct} = 182$ kΩ, $a = 0.895$. Based on the fits to the data of EIS measurement using the Randles circuit, the calculated $C_{DL}\ is$ 746 μF. Thereby, the difference between the double layer capacitance measured using scan rate-dependent CVs (812.5 μF) and EIS (746 μF) is within 15%. Therefore, the enhanced double layer capacitance of the templated nano-mesh electrode compared with previous researches was verified by using these two methods.[36]

3.3 Comparative electrochemical evaluation of the template-guided nano-mesh ion selective (TN-ISE) sensor vs. the SW-CNT ISE sensor

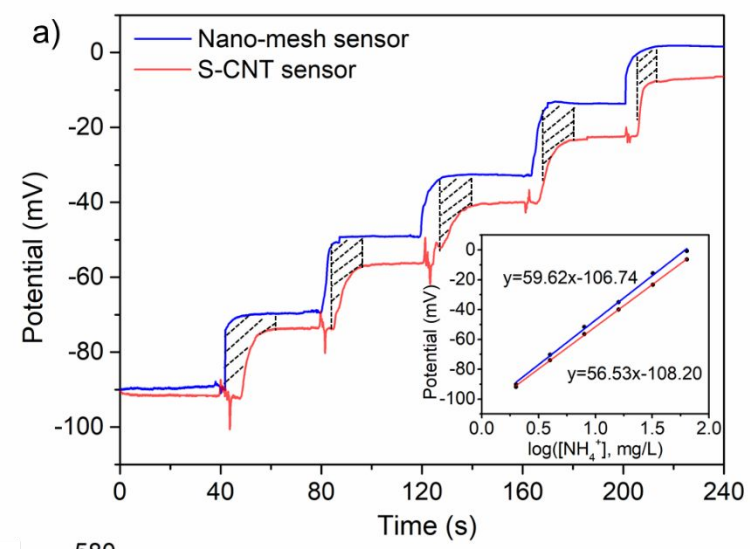
a)
Nano-mesh sensor
S-CNT sensor
Potential (mV)
Time (s)
y=59.62x-106.74
y=56.53x-108.20
log([NH4+], mg/L)

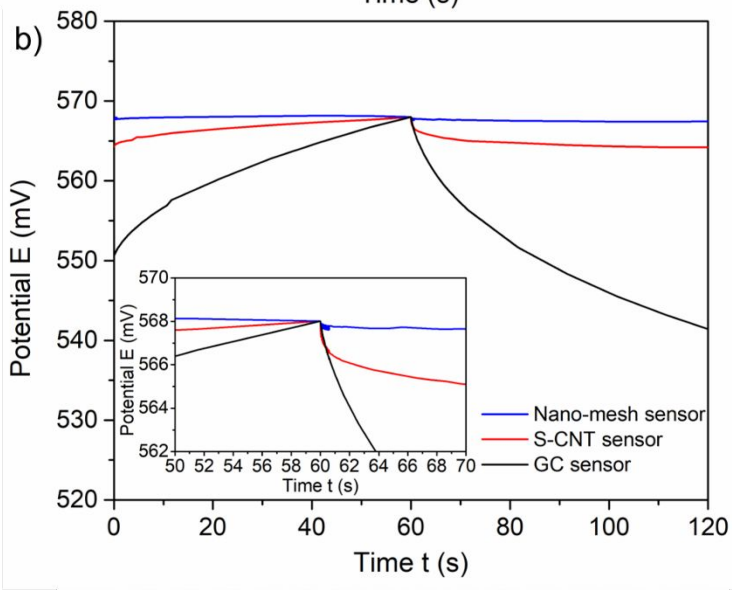
b)
Potential E (mV)
Time t (s)
Nano-mesh sensor
S-CNT sensor
GC sensor

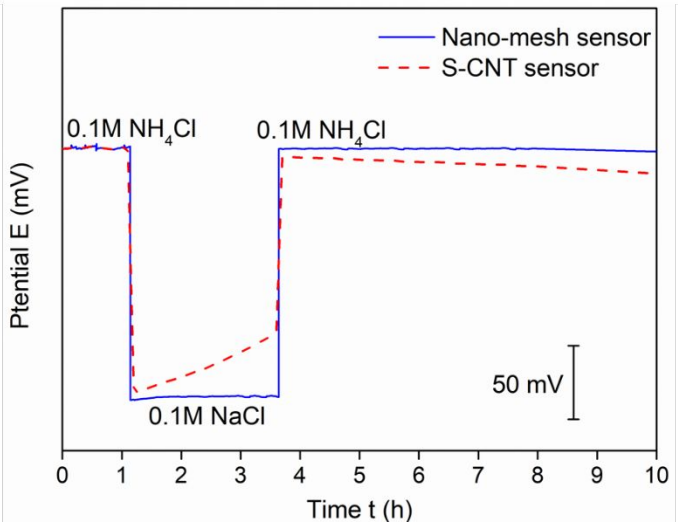
c)
Nano-mesh sensor
S-CNT sensor
0.1M NH4Cl
0.1M NH4Cl
0.1M NaCl
50 mV
Ptential E (mV)
Time t (h)

Figure 3. Electrochemical evaluation of template-guided nano-mesh ion selective electrode (TN-ISE) sensor (a) calibration curve comparison between template-guided nano-mesh ISE sensor and SW-CNT ISE sensor. The grid area is the saved response time; (b) Chronopotentiometry test for nano-mesh ISE sensor (blue line), SW-CNT ISE sensor (red line), and graphite (GC) ISE sensor (black line); (c) Water layer test nano-mesh ISE sensor (blue solid line) and SW-CNT ISE sensor (red dash line). 0.1 M NaCl solution was used for alternating environment solution.

The performance of TN-ISE sensors was compared side-by-side with a TW-CNT ISE sensors in the electrochemical tests. Specifically, rapid response of ISE sensors towards the changes of water quality is critical for early warning and swift control in WTPs and WWTPs. TN-ISE sensors exhibited shorter response time than S-CNT ISE sensors under multiple changes of NH_4^+ concentration (2-64 mg/L in Fig. 3a). This is caused by the lower resistivity (at 20 ℃) of Ni than that of SW-CNT.[41] Also, the slope of the calibration curve representing the sensitivity of the TN-ISE sensor (blue line, 59.62 mV/dec) is higher than the S-CNT ISE sensor (red line, 56.53 mV/dec) and is near the theoretical limiting value (Nernst-slope value of 59 mV/log([NH_4^+]).

The potential (mV) reading stability of the TN-ISE NH_4^+ sensor was examined using constant-current chronopotentiometry, a widely used technique to evaluate the short-term potential stability of ISE sensors.[7, 33] The chronopotentiometry results of the TN-ISE sensor (blue line) were compared with those for the S-CNT ISE sensor (red line) and GC-ISE sensor (black line) under currents of $\pm$ 1 nA (Fig. 3b). The rationale behind this experiment is to challenge the sensor (i.e., with external current of alternating $\pm$ 1 nA) and to assess the response (i.e., reading drift over time $\frac{\Delta E}{\Delta t}$) of the sensor. The obtained reading drift $\frac{\Delta E}{\Delta t}$ (after 60 s) of the TN-ISE sensor was only

5.38 μV/s, a much lower value than obtained for the SW-CNT (11.13 μV/s) and the GC-ISE sensor (448.8 μV/s) (Fig. 3b). The small drift also represents an improvement over previous studies, such as using nano-porous gold (28.3 $\pm$ 8 μV/s)[6], graphene (12.8 μV/s),[42] or tetrathiafulvalene (16.5 μV/s),[43] confirming the superior properties of the TN-ISE sensor. We attribute this to the high electrical double-layer capacitance of the TN electrode (Eq. 1) (Fig. 1g), which could alleviate polarization of electrode over time and enhance the potential (mV) reading stability.[44, 45]

Water invasion into the ISM after the sensor is soaked in an aqueous solution for an extended period of time (e.g., > 2 h) can lead to the presence of a thin water layer between the ISM matrix and the electronic conductor (Fig. 3c).[3, 29, 46] This thin water layer makes the phase boundary potential sensitive to the changes in the ionic content of bulk water solution[30] and causes a steadily varying dynamic equilibrium that subsequently leads to sensor reading drifts over time.[16] In order to prevent the formation of water layers, much effort has been focused on the development of solid contacts with high hydrophobicity,[46, 47] which was assessed using the water contact angle of the solid-contact material. Larger contact angles indicate more hydrophobic materials. The results showed that the contact angle of nano-mesh ISE (~94.69°) was larger than SW-CNT ISE (~80.81 °) (Fig. S1), proving the advanced hydrophobicity of the surface of nano-mesh ISE. Besides this hydrophobicity tests, a water layer test was performed to evaluate the water prevention. Specifically, both TN-ISE and S-CNT ISE sensors were soaked alternately in an aqueous 0.1 M NH_4Cl solution for 1 h, 0.1 M NaCl solution for 2.5 h, and then back in 0.1 M NH_4Cl solution for 6.5h. The TN-ISE sensors showed minimal reading drift throughout the water layer test (Fig. 3c), while the S-CNT ISE sensor exhibited clear reading drifts under the same conditions, suggesting water layer formation,[16, 29] attributed to the random distribution of the S-CNT and the voids

between S-CNT and the ISM matrix (Fig. 1a). Water layer formation test confirmed that the improved hydrophobicity plays an important role in preventing water layer formation.

3.4 Verify the prevention of component leaching in the TN-ISM sensor

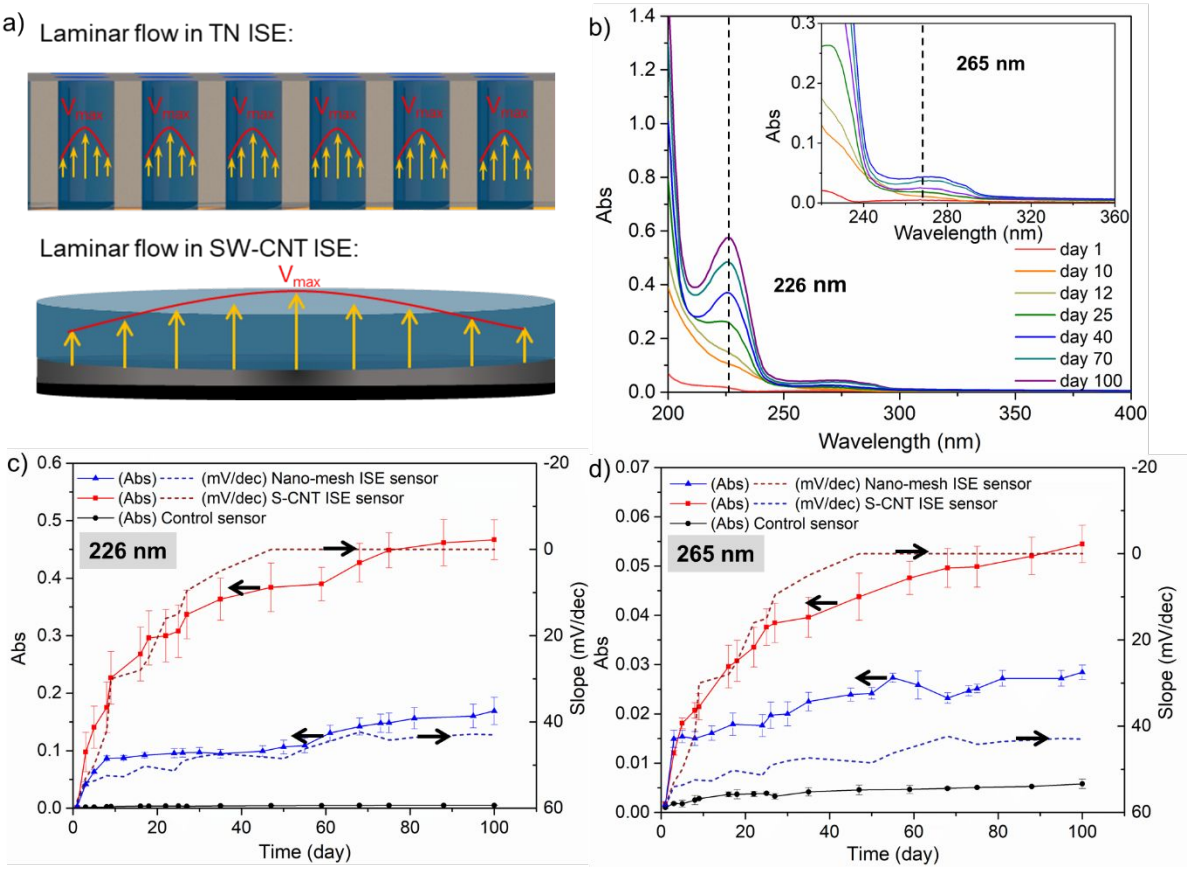

Figure 4. Quantification of the components leaching process by UV-visible spectrophotometry. (a) laminar flow model applied in TN ISE and SW-CNT ISE respectively; (b) Determination of the locations of wavelengths (226 nm and 265 nm) for absorbance peaks using the spectra of DI water solution in which the S-CNT ISE sensor was tested for 100 d. Inset is the enlarged view of spectrum in range around 265 nm; (c)-(d) Comparison of the long-term, time-dependent absorbances observed for TN-ISE sensor and S-CNT ISE sensor immersed in DI water for 100 d

at 226 nm and 265 nm. The error bars are based on triplicate experiments. The dash lines are the sensitivity (slope) change of both types of sensors throughout the 100-day test period.

The lifetime of an ISE electrode may be defined as the time interval between the conditioning of the ion selective membrane and the moment when the functionality characteristics of the device changes detrimentally. One of the common changes is the leaching out of ISE components (e.g., ionophore, anionic additives). General equations for an estimation of the lifetime as limited by the leaching of ISE components are based on Pick's diffusion laws.[48-50] A theoretical lifetime model was established for ISE in previous studies:[48]

$$t_{\mathrm{lim}} = \frac{Kd\partial}{D_{\mathrm{aq}}} \log \frac{c_0}{c_{\mathrm{lim}}} \quad \text{(Eq.5)}$$

where t_{lim} is the lifetime of ISE, D_{aq} is the diffusion coefficient of the component in the aqueous phase, K is the partition/distribution coefficient of the component between the aqueous solution and the membrane, d is the thickness of the ISE membrane, and ∂ is the quantitative descriptions of the effective thickness of the Nernstian diffusion layer. Specifically, ∂ can be obtained from the fundamental theoretical treatment of hydrodynamics:[51]

$$\partial = D_{aq}^{1/3} L^{1/3} R^{1/3} V_{aq}^{-1/3} \quad \text{(Eq.6)}$$

It follows the theory of laminar flow through a tubular membrane system of length (L) and radius (R). Since the nano mesh separates the entire ISM into "n" tubular membrane systems, the final ∂ becomes the sum of each individual ∂:

$$\partial_{\text{sum, nano}-\text{mesh}} = n^{2/3} \cdot D_{aq}^{1/3} L^{1/3} R^{1/3} V_{aq}^{-1/3} \quad \text{(Eq.7)}$$

Thus, the $\partial_{\text{sum, nano}-\text{mesh}}$ is far larger than the common ∂ (e.g., SW-CNT), leading to a considerably extended lifetime of TN ISE and a minimized leaching out process, which could also

be described by laminar flow models in TN ISE and SW-CNT ISE (Fig. 4a). It illustrates the leaching out of components with a slower velocity since the flowing tube is way narrower in nano mesh than in wide-open ISM. This theory was proved by the following experiment results using UV-Vis spectroscopy.

The leaching process of lipophilic anionic additives (e.g. tetrakis(4-chlorophenyl)borate, KT4ClPB) from ISE membrane matrix to bulk aqueous solution causes adverse effects on the detection limit and the sensitivity of ISE sensors.[50, 52, 53] In this study, the leaching process was quantified using the UV-vis absorption of KT4ClPB. Based on the functional groups present (Fig. S2 and S3) the bands at 226 nm and 265 nm were used to quantify the leaching amount of KT4ClPB from the ISE sensors.[54, 55] The similar phenomenon was found when we tested the leaching process over the whole ISE sensors (with polymer phase) (Fig. 4b). For the S-CNT ISE sensors immersed in DI water, the steadily increasing absorbance over time (100 d) proved the constant leaching of KT4ClPB to the bulk aqueous solution. The rate of increase in absorbance at 226 nm corresponded to rate observed at 265 nm (inset, Fig. 4b). Thus, the evaluation of the changes at both wavelengths provides an excellent evaluation criterion for lipophilic salt leaching.

In comparison, the leaching process of the novel TN-ISE sensors were also examined in DI water for 100 days. Since the initial concentration of KT4ClPB in both sensors were same, the relative lower terminal absorption values at 226 and 265 nm at the end of the test period demonstrated a strong mitigation of the leaching process (Fig. 4c and 4d). We attribute this to the ions being locked within the nano-mesh. Adsorption is usually an effect of van der Waals and other electrostatic forces.[56] By trapping the functional substances inside the electrode matrix, the long-term stability of TN-ISE sensors is assured. In contrast, components like KT4ClPB can more readily leaches out of the ISM matrix membrane because of its loose contact interface with S-CNT.

The broken lines in Fig. 4c and 4d show that the sensor sensitivity (slope) declined along with the KT4ClPB leaching process. The slope of the S-CNT ISE sensor declined to 0 mV/dec at around 50 d, illustrating that the sensor had stopped working. In comparison, the slope of the TN-ISE sensor declined only slightly and still returned 40 mV/dec after 100 d. This result underlines the importance of minimizing the leaching of lipophilic salts from the ISM polymer matrix and confirms that nano-mesh structure enhanced the long-term sensor reading stability. More importantly, these experimental results are consistent with the theoretical model and further prove that the nano mesh structure can effectively mitigate the leaching process and extend the lifetime of ISE sensors.

3.5 Long-term continuous monitoring of wastewater quality using the TN-ISE sensor

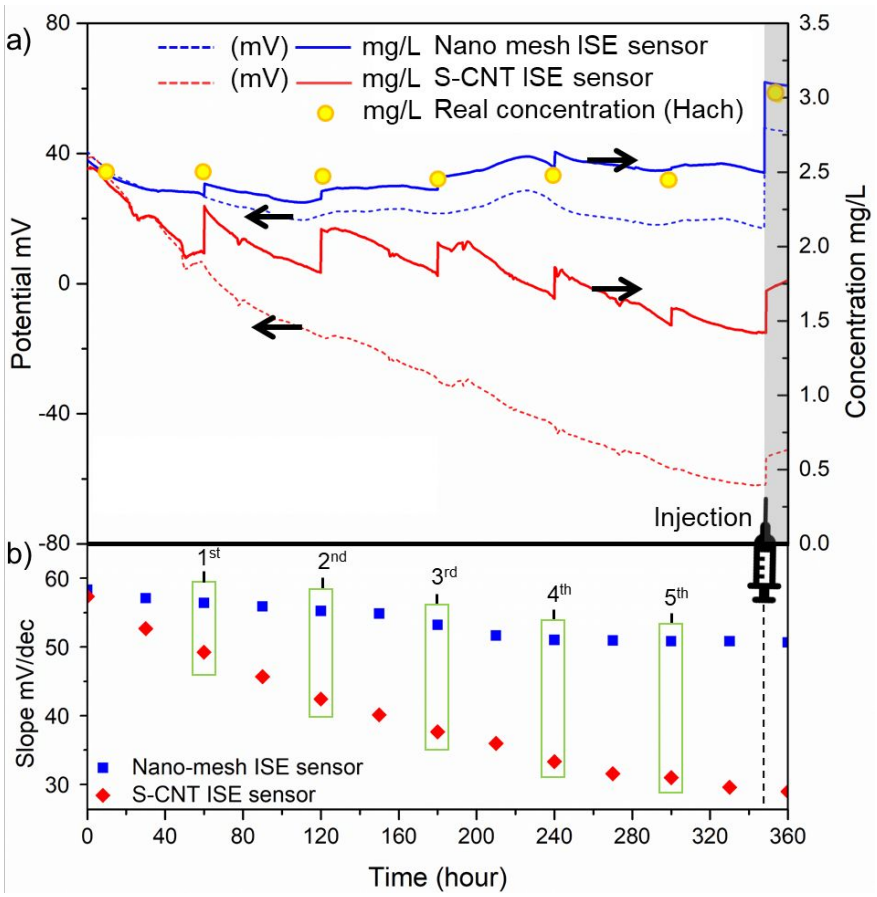

Figure 5. (a) Continuous long-term (360 h) tests of the TN ISE sensor (blue dash line) and the S-CNT ISE sensor (red dash line) in wastewater. The blue and red solid line represents the converted concentration (mg/L) through potentiometric readings. The yellow circle represents the real concentration obtained by Hach instrument. (b) The slope changes of TN-ISE and S-CNT ISE sensors during 360 h. Five slope values were used to calibrate these sensors. The shock was injected at the 350th hour.

Table 1. NH_4^+ concentration of wastewater validated using Hach DR2800 (sampled at 0, 60, 120, 180, 240, 300, and 350 h) and compared with the results obtained using the TN ISE and S-CNT ISE sensors.

	0	60h	120h	180h	240h	300h	350h	Average error
Hach DR2800	2.50	2.48	2.49	2.46	2.48	2.45	3.00	-
Nano-mesh ISE sensor	2.58	2.42	2.37	2.47	2.63	2.53	3.08	1.28%
	3.2%	2.4%	4.7%	0.5%	6.2%	3.3%	2.8%	
S-CNT ISE sensor	2.52	2.27	2.11	2.02	1.86	1.58	1.75	20.35%
	1.0%	8.5%	15.1%	17.8%	25.0%	35.4%	41.6%	

The side-by-side performance of the TN ISE and S-CNT ISE sensors with respect to the continuous monitoring of NH_4^+ concentration over 360 h (15 days) was also compared in wastewater. The NH_4^+ concentration in the wastewater (~2.5 mg/L) was validated using the Hach DR2800 method (yellow circle in Fig. 5a). Based on the constant NH_4^+ concentration in wastewater throughout the test period, the microbial activity in wastewater was inhibited. The TN-ISE sensor exhibited a smaller reading drift in wastewater (blue solid line: 22 mV/350 h) than the S-CNT ISE sensor (red dashed line: 99 mV/350 h) (Fig. 5a). We attribute this higher stability by the enhanced capacitance of the nano-mesh electrode and the compact contact interface between electrode and ISM matrix (Fig 1g, Fig. 3c, Fig. 4c and 4d).

One approach to compensate for the potential (mV) reading drift is an intermittent reading compensation based on the sensor slope (i.e. sensitivity, mV/dec).[2, 7, 8] Thus, the slope change of the sensors over time was calculated for compensation (Fig. 5a). Five times intermittent compensation in total were implemented during the 350 h test period. However, despite these corrections, there was still a large discrepancy (with an average discrepancy of 20%, Table 1) between the NH_4^+ concentration readings of the S-CNT ISE sensor and the concentration value

validated by the HACH method. In contrast, the average error caused by the TN ISE sensor was quite low and fixed to 1.28% (Table 1), again identifying this sensor as the superior system. We attribute the smaller reading drift of the TN-ISE to the mechanical stability of the nano mesh structure in wastewater. In previous studies, ideal condition (e.g., 0.1 M KCl solution) were applied in long-term application to evaluate any reading drift.[3, 7, 30] However, in wastewater, the sensors are exposed to a number of other ions and suspended particles. In addition, the turbulence because of the constant stirring was a mechanical stress factor, especially in longer time duration. In this study, the interface between SW-CNT as solid contact and the ISM were disturbed due to the suspension and turbulence gradually leading to an early water layer formation and failure. On the other hand, the electrodeposition of the nano-mesh along with ISM matrix produced a compact and mechanically and chemically robust interface that prevented water layer formation, ultimately leading to superior potential (mV) reading stability.

Furthermore, after being immersed in wastewater for 350 h, shock solutions (2.5 mg/L to 3.0 mg/L) were added to the wastewater in order to assess the sensitivity of the ISE sensors after an extended time of use. A higher potential (mV) response by the TN ISE sensor (~31 mV) than S-CNT ISM sensor (~8 mV) was exhibited (Fig. 5a). This is consistent with our leaching test that revealed that a higher potential (mV) response was associated with a better entrapment of KT4ClPB in the ISE polymer matrix in the TN ISE sensor (Fig 4c and 4d). Thereby, the sensor sensitivity (slope) of the TN-ISC sensor declined over time slower and was maintained at a relatively high value (50.8 mV/dec), while the sensitivity of S-CNT ISE sensor leaching KT4ClPB from the ISE polymer matrix faster steadily dropped to 30.9 mV/dec (Fig. 5b). A stable sensitivity over time is more appropriate for intermittent reading correction and enhanced sensors' accuracy for long-term monitoring in wastewater.

3.6 Outlook of Using Nano-mesh ISE Sensor for Long-Term Continuous Monitoring of Water Quality

Nano materials such as carbon nanotube, graphene, metallic nano particles, and nano wires have been widely applied in ion selective electrode sensors due to their large interface area, large capacitance and excellent conductivity.[12, 20] However, the commonly used approach of incorporating these nano-materials into ion selective membrane has been limited to mechanical joints and mixing,[7, 57] leading to problems such as water uptake/penetration, polymer material detachment, and ion selective membrane components leaching out. In this study, the AAO template-guided technique was used for trapping/immobilizing ion selective membrane inside the nano materials (e.g., nano mesh), enhancing its electrochemical stability. This drastically prolonged the lifespan of the sensor. This study unveils an original direction for the utilization of nanomaterials in ISE sensor fabrication for real-world applications.

Although the template-guided nano-mesh ISE (TN-ISE) sensors exhibited better performance than regular single wall carbon nanotube (SW-CNT ISE) sensors in both characterization test and long-term wastewater test, more efforts are needed to optimize the TN-ISE sensor. For example, several critical parameters of the nano-mesh not investigated here in this proof-of-principle study are deemed critical for the development of the sensor; these include the optimal surface roughness of the substrate, the depth of the internal tube space of nano-mesh, and the thickness of the imprinting substrate (Al foil). Furthermore, other experimental parameters (e.g., the conditions for the first/second-anodization, electrodeposition, and etching processes, etc.) can perceivably be adjusted to further improve the accuracy and stability of the TN-ISE sensors. Nickel was used as the electrode substrate in this study. However, other advanced alloys or bimetals could be examined in future studies to enhance the sensor performance. Lastly, the coating of the nano-

mesh electrodes with an ion-permeable antifouling protection layer (e.g., non-stick coatings , biocide coatings, etc.[58, 59]) could be another strategy to further prolong the sensor lifespan in wastewater.

Conclusion

We introduce a novel template-guided nano-mesh fabrication technique to immobilize the ion selective membrane (ISM) inside the membrane polymer matrix. This technology achieved a NH_4^+-specific sensor suitable for the long-term continuous monitoring of water and wastewater quality. By using the template-guided nano-mesh fabrication technique, the contact surface between ion selective membrane (ISM) and the Ni electrode was compact enough to fundamentally solve the water invasion problem, the capacitance of the TN-ISE sensor was enormously enhanced, and this chemosensor immobilization process substantially retarded ISM components leaching. As a direct consequence of these improvements, the template-guided nano-mesh ion selective electrode (TN-ISE) sensor exhibited a much higher potential (mV) reading stability than traditional carbon nanotube (CNT) based sensors during long-term (100 days) application in water, a considerable improvement over the lifespan for existing drop-cast S-ISE sensors of 2-10 days.[2,8, 60] The template-guided technique for membrane immobilization developed in this study establishes a platform for the fabrication of ISE sensors with broad applications in water and wastewater.

Acknowledgement

This study was supported by National Science Foundation (NSF) Environmental Engineering Program GOALI Project (Grant No.: 1706343), NSF Partnerships for Innovation (PFI) Accelerate Innovative Research (AIR) Project (Grant No: 1640701), NSF I-Corps Project (Grant No:

1655451), NSF Smart and Connected Communities (SCC) Project (Grant No: ECCS- 2018492), Connecticut SPARK Program, and U.S. - Egypt Science and Technology Joint Fund (Grant No. 2000009132). Any opinions, findings, and conclusions or recommendations expressed in this material are those of the authors and do not necessarily reflect the views of the National Science Foundation.

Reference

1. R. Holmes, J. W. McClelland, D. M. Sigman, B. Fry and B. Peterson, Measuring 15N–NH4+ in marine, estuarine and fresh waters: an adaptation of the ammonia diffusion method for samples with low ammonium concentrations, *Marine Chemistry*, 1998, **60**, 235-243.
2. R. Athavale, I. Kokorite, C. Dinkel, E. Bakker, B. Wehrli, G. n. A. Crespo and A. Brand, In Situ Ammonium Profiling Using Solid-Contact Ion-Selective Electrodes in Eutrophic Lakes, *Analytical Chemistry*, 2015, **87**, 11990-11997.
3. J. Hu, A. Stein and P. Bühlmann, Rational design of all-solid-state ion-selective electrodes and reference electrodes, *TrAC Trends in Analytical Chemistry*, 2016, **76**, 102-114.
4. E. Bakker, P. Bühlmann and E. Pretsch, Carrier-based ion-selective electrodes and bulk optodes. 1. General characteristics, *Chemical Reviews*, 1997, **97**, 3083-3132.
5. J. Bobacka, A. Ivaska and A. Lewenstam, Potentiometric ion sensors, *Chemical Reviews*, 2008, **108**, 329-351.
6. T. Yin, D. Pan and W. Qin, All-solid-state polymeric membrane ion-selective miniaturized electrodes based on a nanoporous gold film as solid contact, *Analytical Chemistry*, 2014, **86**, 11038-11044.
7. X. Chen, G. Zhou, S. Mao and J. Chen, Rapid detection of nutrients with electronic sensors: a review, *Environmental Science: Nano*, 2018, **5**, 837-862.
8. Y. Huang, T. Wang, Z. Xu, E. Hughes, F. Qian, M. Lee, Y. Fan, Y. Lei, C. Brückner and B. Li, Real-Time in Situ Monitoring of Nitrogen Dynamics in Wastewater Treatment Processes using Wireless, Solid-State, and Ion-Selective Membrane Sensors, *Environmental Science & Technology*, 2019, **53**, 3140-3148.
9. P. L. McCarty, What is the best biological process for nitrogen removal: when and why? *Journal*, 2018, **52**, 3835-3841.
10. R. P. Buck and E. Lindner, Recommendations for nomenclature of ionselective electrodes (IUPAC Recommendations 1994), *Pure and Applied Chemistry*, 1994, **66**, 2527-2536.
11. C. W. Outhwaite, S. Lamperski and L. B. Bhuiyan, Influence of electrode polarization on the capacitance of an electric double layer at and around zero surface charge, *Molecular Physics*, 2011, **109**, 21-26.
12. Y. Xie, D. Kocaefe, C. Chen and Y. Kocaefe, Review of research on template methods in preparation of nanomaterials, *Journal of Nanomaterials*, 2016, **2016**.
13. R. Hernández, J. Riu and F. X. Rius, Determination of calcium ion in sap using carbon nanotube-based ion-selective electrodes, *Analyst*, 2010, **135**, 1979-1985.
14. F. Li, J. Ye, M. Zhou, S. Gan, Q. Zhang, D. Han and L. Niu, All-solid-state potassium-selective electrode using graphene as the solid contact, *Analyst*, 2012, **137**, 618-623.
15. R. De Marco, J.-P. Veder, G. Clarke, A. Nelson, K. Prince, E. Pretsch and E. Bakker, Evidence of a water layer in solid-contact polymeric ion sensors, *Physical Chemistry Chemical Physics*, 2008, **10**, 73-76.
16. M. Fibbioli, W. E. Morf, M. Badertscher, N. F. de Rooij and E. Pretsch, Potential drifts of solid-contacted ion-selective electrodes due to zero-current ion fluxes through the sensor membrane, *Electroanalysis*, 2000, **12**, 1286-1292.
17. Z. Fan, R. Kapadia, P. W. Leu, X. Zhang, Y.-L. Chueh, K. Takei, K. Yu, A. Jamshidi, A. A. Rathore and D. J. Ruebusch, Ordered arrays of dual-diameter nanopillars for maximized optical absorption, *Nano Letters*, 2010, **10**, 3823-3827.
18. T. Ozel, G. R. Bourret and C. A. Mirkin, Coaxial lithography, *Nature Nanotechnology*, 2015, **10**, 319.

19. Y. Mi, L. Wen, R. Xu, Z. Wang, D. Cao, Y. Fang and Y. Lei, Constructing a AZO/TiO_2 core/shell nanocone array with uniformly dispersed Au NPs for enhancing photoelectrochemical water splitting, *Advanced Energy Materials*, 2016, **6**, 1501496.
20. L. Wen, R. Xu, Y. Mi and Y. Lei, Multiple nanostructures based on anodized aluminium oxide templates, *Nature Nanotechnology*, 2017, **12**, 244.
21. H. Masuda, A. Abe, M. Nakao, A. Yokoo, T. Tamamura and K. Nishio, Ordered mosaic nanocomposites in anodic porous alumina, *Advanced Materials*, 2003, **15**, 161-164.
22. T. Yanagishita, M. Sasaki, K. Nishio and H. Masuda, Carbon Nanotubes with a Triangular Cross-section, Fabricated Using Anodic Porous Alumina as the Template, *Advanced Materials*, 2004, **16**, 429-432.
23. T. Wang, Z. Xu, Y. Huang, Z. Dai, X. Wang, M. Lee, C. Bagtzoglou, C. Brückner, Y. Lei and B. Li, Real-time in situ auto-correction of K^+ interference for continuous and long-term NH_4^+ monitoring in wastewater using solid-state ion selective membrane (S-ISM) sensor assembly, *Environmental Research*, 2020, **189**, 109891.
24. Y. Fan, Z. Xu, Y. Huang, T. Wang, S. Zheng, A. DePasquale, C. Brüeckner, Y. Lei and B. Li, Long-term continuous and real-time in situ monitoring of Pb(II) toxic contaminants in wastewater using solid-state ion selective membrane (S-ISM) Pb and pH auto-correction assembly, *Journal of Hazardous Materials*, 2020, **400**, 123299.
25. C.-Z. Lai, M. A. Fierke, A. Stein and P. Bühlmann, Ion-selective electrodes with three-dimensionally ordered macroporous carbon as the solid contact, *Analytical Chemistry*, 2007, **79**, 4621-4626.
26. J. Hu, X. U. Zou, A. Stein and P. Bühlmann, Ion-selective electrodes with colloid-imprinted mesoporous carbon as solid contact, *Analytical Chemistry*, 2014, **86**, 7111-7118.
27. E. Bakker, E. Pretsch and P. Bühlmann, Selectivity of potentiometric ion sensors, *Analytical Chemistry*, 2000, **72**, 1127-1133.
28. J. Zhu, Y. Qin and Y. Zhang, Preparation of all solid-state potentiometric ion sensors with polymer-CNT composites, *Electrochemistry Communications*, 2009, **11**, 1684-1687.
29. G. A. Crespo, S. Macho and F. X. Rius, Ion-selective electrodes using carbon nanotubes as ion-to-electron transducers, *Analytical Chemistry*, 2008, **80**, 1316-1322.
30. C. R. Rousseau and P. Bühlmann, Calibration-free potentiometric sensing with solid-contact ion-selective electrodes, *TrAC Trends in Analytical Chemistry*, 2021, **140**, 116277.
31. J. Shang, L. Liu, R. Yang and P. Zhang, Anodic aluminum oxide template with large area and small holes prepared by gradual voltage-rising method, *Nanotechnology and Precision Engineering*, 2008, **6**, 322-326.
32. K. Liu, J. Chen, L. Zhou, L. Zhang and Y. Fang, Fabrication of high quality ordered porous anodic aluminum oxide templates, *High Power Laser and Particle Beams*, 2010, **22**, 1531-1534.
33. J. Bobacka, Potential stability of all-solid-state ion-selective electrodes using conducting polymers as ion-to-electron transducers, *Analytical Chemistry*, 1999, **71**, 4932-4937.
34. S. Zhao, H. Roberge, A. Yelon and T. Veres, New application of AAO template: a mold for nanoring and nanocone arrays, *Journal of the American Chemical Society*, 2006, **128**, 12352-12353.
35. G. Kawamura, H. Muto and A. Matsuda, Hard template synthesis of metal nanowires, *Frontiers in Chemistry*, 2014, **2**, 104.
36. C. C. McCrory, S. Jung, J. C. Peters and T. F. Jaramillo, Benchmarking heterogeneous electrocatalysts for the oxygen evolution reaction, *Journal of the American Chemical Society*, 2013, **135**, 16977-16987.
37. S. Trasatti and O. Petrii, Real surface area measurements in electrochemistry, *Pure and Applied Chemistry*, 1991, **63**, 711-734.
38. R. Boggio, A. Carugati and S. Trasatti, Electrochemical surface properties of Co_3O_4 electrodes, *Journal of Applied Electrochemistry*, 1987, **17**, 828-840.

39. M. E. Orazem and B. Tribollet, Electrochemical Impedance Spectroscopy, John Wiley & Sons, *New Jersey*, 2017.
40. G. Brug, A. L. van den Eeden, M. Sluyters-Rehbach and J. H. Sluyters, The analysis of electrode impedances complicated by the presence of a constant phase element, *Journal of Electroanalytical Chemistry and Interfacial Electrochemistry*, 1984, **176**, 275-295.
41. Y. T. Ong, A. L. Ahmad, S. H. S. Zein and S. H. Tan, A review on carbon nanotubes in an environmental protection and green engineering perspective, *Brazilian Journal of Chemical Engineering*, 2010, **27**, 227-242.
42. J. Ping, Y. Wang, J. Wu and Y. Ying, Development of an all-solid-state potassium ion-selective electrode using graphene as the solid-contact transducer, *Electrochemistry Communications*, 2011, **13**, 1529-1532.
43. M. Pięk, R. Piech and B. Paczosa-Bator, Improved nitrate sensing using solid contact ion selective electrodes based on TTF and its radical salt, *Journal of The Electrochemical Society*, 2015, **162**, B257.
44. R. Burt, G. Birkett and X. Zhao, A review of molecular modelling of electric double layer capacitors, *Physical Chemistry Chemical Physics*, 2014, **16**, 6519-6538.
45. M. V. Fedorov, N. Georgi and A. A. Kornyshev, Double layer in ionic liquids: The nature of the camel shape of capacitance, *Electrochemistry Communications*, 2010, **12**, 296-299.
46. T. Lindfors, F. Sundfors, L. Höfler and R. E. Gyurcsányi, FTIR - ATR Study of Water Uptake and Diffusion Through Ion - Selective Membranes Based on Plasticized Poly (vinyl chloride), *Electroanalysis*, 2009, **21**, 1914-1922.
47. T. Lindfors and A. Ivaska, Stability of the inner polyaniline solid contact layer in all-solid-state K+-selective electrodes based on plasticized poly (vinyl chloride), *Analytical Chemistry*, 2004, **76**, 4387-4394.
48. O. Dinten, U. E. Spichiger, N. Chaniotakis, P. Gehrig, B. Rusterholz, W. E. Morf and W. Simon, Lifetime of neutral-carrier-based liquid membranes in aqueous samples and blood and the lipophilicity of membrane components, *Analytical Chemistry*, 1991, **63**, 596-603.
49. W. E. Morf, K. Seiler, B. Lehmann, C. Behringer, K. Hartman and W. Simon, Carriers for chemical sensors: design features of optical sensors (optodes) based on selective chromoionophores, *Pure and Applied Chemistry*, 1989, **61**, 1613-1618.
50. M. Telting-Diaz and E. Bakker, Effect of lipophilic ion-exchanger leaching on the detection limit of carrier-based ion-selective electrodes, *Analytical Chemistry*, 2001, **73**, 5582-5589.
51. V. G. Levich, Physicochemical hydrodynamics prentice-hall, Prentice Hall*, New Jersey*, 1962.
52. P. Bühlmann, E. Pretsch and E. Bakker, Carrier-based ion-selective electrodes and bulk optodes. 2. Ionophores for potentiometric and optical sensors, *Chemical Reviews*, 1998, **98**, 1593-1688.
53. E. Bakker and E. Pretsch, Lipophilicity of tetraphenylborate derivatives as anionic sites in neutral carrier-based solvent polymeric membranes and lifetime of corresponding ion-selective electrochemical and optical sensors, *Analytica Chimica Acta*, 1995, **309**, 7-17.
54. M. A. Marzouk, S. M. Abo-Naf, H. A. Zayed and N. S. Hassan, Photoluminescence and semiconducting behavior of Fe, Co, Ni and Cu implanted in heavy metal oxide glasses, *Journal of Materials Research and Technology*, 2016, **5**, 226-233.
55. S. S. Gujral, UV-Visible spectral analysis of boric acid in different solvents: a case study, *International Journal of Pharmaceutical Sciences and Research*, 2015, **6**, 830.
56. D. S. Raja, W.-L. Liu, H.-Y. Huang and C.-H. Lin, Immobilization of protein on nanoporous metal-organic framework materials, *Comments on Inorganic Chemistry*, 2015, **35**, 331-349.
57. G. n. A. Crespo, S. Macho, J. Bobacka and F. X. Rius, Transduction mechanism of carbon nanotubes in solid-contact ion-selective electrodes, *Analytical Chemistry*, 2008, **81**, 676-681.

58. P.-H. Lin and B.-R. Li, Antifouling strategies in advanced electrochemical sensors and biosensors, *Analyst*, 2020, **145**, 1110-1120.
59. A. Delgado, C. Briciu-Burghina and F. Regan, Antifouling Strategies for Sensors Used in Water Monitoring: Review and Future Perspectives, *Sensors*, 2021, **21**, 389.
60. B. Paczosa-Bator, R. Piech and A. Lewenstam, Determination of the leaching of polymeric ion-selective membrane components by stripping voltammetry, *Talanta*, 2010, **81**, 1003-1009.